J. Marine Sci. Appl. (2016) 15: 123-135
DOI: 10.1007/s11804-016-1358-6

Hydrodynamic Performance of Multiple-Row Slotted Breakwaters

Moussa S. Elbisy[1*], Ehab M. Mlybari[2] and Medhat M. Helal[3]

1. Civil Engineering Department, Higher Technological Institute, Tenth of Ramadan City 44629, Egypt
2. Civil Engineering Department, Umm Al-Qura University, Makkah 21955, Saudi Arabia
3. Department of Engineering Mathematics and Physics, Zagazig University, Zagazig 44511, Egypt

Abstract: This study examines the hydrodynamic performance of multiple-row vertical slotted breakwaters. We developed a mathematical model based on an eigenfunction expansion method and a least squares technique for Stokes second-order waves. The numerical results obtained for limiting cases of double-row and triple-row walls are in good agreement with results of previous studies and experimental results. Comparisons with experimental measurements of the reflection, transmission, and dissipation coefficients (C_R, C_T, and C_E) for double-row walls show that the proposed mathematical model adequately reproduces most of the important features. We found that for double-row walls, the C_R increases with increasing wave number, *kd*, and with a decreasing permeable wall part, *dm*. The C_T follows the opposite trend. The C_E slowly increases with an increasing *kd* for lower *kd* values, reaches a maximum, and then decreases again. In addition, an increasing porosity of *dm* would significantly decrease the C_R, while increasing the C_T. At lower values of *kd*, a decreasing porosity increases the C_E, but for high values of *kd*, a decreasing porosity reduces the C_E. The numerical results indicate that, for triple-row walls, the effect of the arrangement of the chamber widths on hydrodynamic characteristics is not significant, except when $kd<0.5$. Double-row slotted breakwaters may exhibit a good wave-absorbing performance at $kd>0.5$, where by the horizontal wave force may be smaller than that of a single wall. On the other hand, the difference between double-row and triple-row vertical slotted breakwaters is marginal.

Keywords: slotted breakwaters, Stokes second-order waves, transmission coefficient, reflection coefficient, dissipation coefficient, horizontal wave force

Article ID: 1671-9433(2016)02-0123-13

1 Introduction

The development and use of coastal regions play an important role in the national income of many countries worldwide. Coastal regions are a source of attraction for many human activities. Major concerns associated with these regions include the protection of the coastal area, harbors, and marinas and the use of methods that have the fewest side effects on the adjacent and neighboring shores, are most environmentally friendly, and are as inexpensive as possible.

There are many types of coastal protection structures, including artificial beaches, breakwaters, jetties, seawalls, artificial headlands, and groins. Breakwaters are commonly used along shorelines, channel entrances, beaches, harbors, or marinas. The main function of a breakwater is to provide shore protection by controlling the wave height and current velocity that may be transmitted along the coast and inside harbors. Breakwaters are classified according to their degree of protection: full and partial protection breakwaters. Full protection breakwaters are most commonly used and are known as conventional breakwaters, although they have inherent drawbacks such as being massive, environmentally harmful, causing excessive reflections, and not being economical in deeper water. Partial protection, or nonconventional, breakwaters have been used more recently and have been shown to overcome the limitations of conventional breakwaters (Tsinker, 1995).

There are many types of partial protection breakwaters, including pneumatic and hydraulic, submerged, floating, flexible floating, detached, perforated, pile, pipe, and slotted breakwaters. The flow behavior through slotted breakwaters is complicated and requires further study to determine its hydrodynamic characteristics and performance efficiency in response to waves. When an array of slotted walls with more than one row is used, the situation becomes even more complicated. The wave interaction with such structures is quite complex; therefore, researchers have conducted experimental and theoretical investigations for understanding flow behavior through a group of slotted walls (Gardner and Townend, 1988; Galal, 2002).

Several studies have proposed configurations of slotted breakwaters to improve their performance and to examine their hydrodynamic influence in attenuating incident waves. In particular, great attention has been given to the development of different geometric configurations. Various numerical model studies have been conducted to better understand the physical behavior of breakwaters.

Kriebel (1992) theoretically and experimentally studied the wave transmission coefficient (C_T) and acting wave forces (F) for a vertical slotted breakwater. The author developed a simple formula for estimating the C_T and F that

Received date: 2015-10-03
Accepted date: 2015-12-28
***Corresponding author Email:** mselbisy@uqu.edu.sa

mainly depends on losses from the gap between the slots.

Isaacson *et al*. (1998, 1999) presented a numerical calculation based on Stokes first-order theory for wave interaction and an eigenfunction expansion method for a single and paired thin vertical slotted barrier extending from the water's surface to a given distance above the seabed. Comparisons between experimental measurements of the transmission, reflection, and dissipation coefficients for this partially submerged slotted barrier exhibited good agreement, indicating that this numerical method adequately accounts for the energy dissipated by the barrier.

Using linear wave theory and eigenfunction expansion, Zhu and Chwang (2001) also studied the interaction between waves and a slotted breakwater. Their research showed that the reflection characteristics of a slotted sea wall mainly depend on the porosity "ε", the primary variable defining the structure permeability of the slotted plate, and the incident wave height. Analytical models based on potential flow for predicting wave reflection from a perforated-wall caisson breakwater have been developed by Suh *et al*. (2001), who also conducted laboratory experiments for irregular waves with various significant wave heights and chamber widths. The authors concluded that the reflected wave spectrum exhibits frequency-dependent oscillatory behavior, and the present study is a modification of their model.

Balaji and Sundar (2004) studied horizontal slotted wave screens with circular intercepting elements and compared their experimental results with those of a numerical model based on Green's identity formula with respect to the effects of porosity and the shape of the intercepting elements.

Suh *et al*. (2006, 2007) described the hydrodynamic characteristics of pile-supported vertical wall breakwaters with circular and square piles under regular and random waves. They used the eigenfunction expansion method for their analysis and estimated the reflection, transmission, run-up, and wave forces acting on the breakwater. This method was further extended to include random waves.

By extending the study of Suh *et al*. (2006), Ji and Suh (2010) developed a mathematical model that can compute various hydrodynamic characteristics of a multiple-row curtainwall–pile breakwater and conducted laboratory experiments for double- and triple-row breakwaters. The results indicated that their mathematical model adequately reproduced most of the important features of the experimental results.

Koraim (2011) theoretically and experimentally investigated one row of a vertical slotted breakwater under normal regular waves and developed a simple theoretical model based on an eigenfunction. He examined the validity of the theoretical model by comparing its results with the theoretical and experimental results obtained from other studies. He found that the transmission coefficient decreases with increasing values of a dimensionless wave number, increasing wave steepness, and decreasing breakwater porosity. He concluded that his theoretical model can be used to predict the performance of slotted breakwaters and the hydrodynamic forces exerted on these structures using the friction coefficient $f=1.5$.

Ahmed *et al*. (2011) developed a numerical model based on an eigenfunction expansion method for regular linear wave interactions with a single and double vertical slotted wall and nonlinear (Stokes second-order) wave interactions with a single vertical slotted wall. They validated the numerical model by comparing its results with those of previous studies and their own experimental results. The authors found that f and the coefficient of porosity ε significantly influence the reflection (C_R), transmission (C_T), and wave energy dissipation (C_E) coefficients of permeable breakwaters, while the influence of the added mass coefficient (C_m) is minimal and can be omitted for this configuration.

The objective of the present study was to describe the flow behavior and the hydraulic performance of multiple-row vertical slotted breakwaters. We developed a mathematical model of Stokes second-order waves based on an eigenfunction expansion method and a least squares technique for wave interaction with multiple-row vertical slotted breakwaters.

2 Theoretical formulation and assumptions

In this section, we describe the mathematical model developed, which is based on an eigenfunction expansion method and a least squares technique. Let's consider the multi-row irregular vertical slotted breakwaters diagrammed in Fig. 1, in which d=constant water depth, du_j is the height of the jth curtainwall below the still water level, dm_j is the draft of the permeable intermediate part of the jth wall, and b_j is the thickness of the jth wall. We defined a Cartesian coordinate system (x and z) with the positive x directed from left to right from a point on the first wall and the vertical coordinate z measured vertically upward from the water line. The center of the jth wall is located at $x=x_j$.

The water wave problem has a free surface boundary that moves with the water particle velocity. This velocity is one of the unknown variables. Therefore, the position of the free surface boundary is also an unknown variable before computation. The fluid domain is divided into J+1 regions by the J walls. The up-wave and down-wave regions of the jth wall are defined as Ω_{j-1} and Ω_j, respectively. Assuming incompressible fluid and irrotational flow motion, the velocity potential exists, which satisfies the Laplace equation. The following boundary value problem is obtained for the velocity potential $\Phi_j(x, z, t)$ in each region:

$$\frac{\partial^2\Phi_j}{\partial x^2}+\frac{\partial^2\Phi_j}{\partial z^2}=0 \quad \text{for} \quad j=0,1,2,...,J \tag{1}$$

$$\frac{\partial\Phi_j}{\partial z}+\frac{1}{g}\frac{\partial^2\Phi_j}{\partial t^2}=0\,, \quad \text{at } z=0 \ \text{ for } \quad j=0,1,2,...,J \tag{2}$$

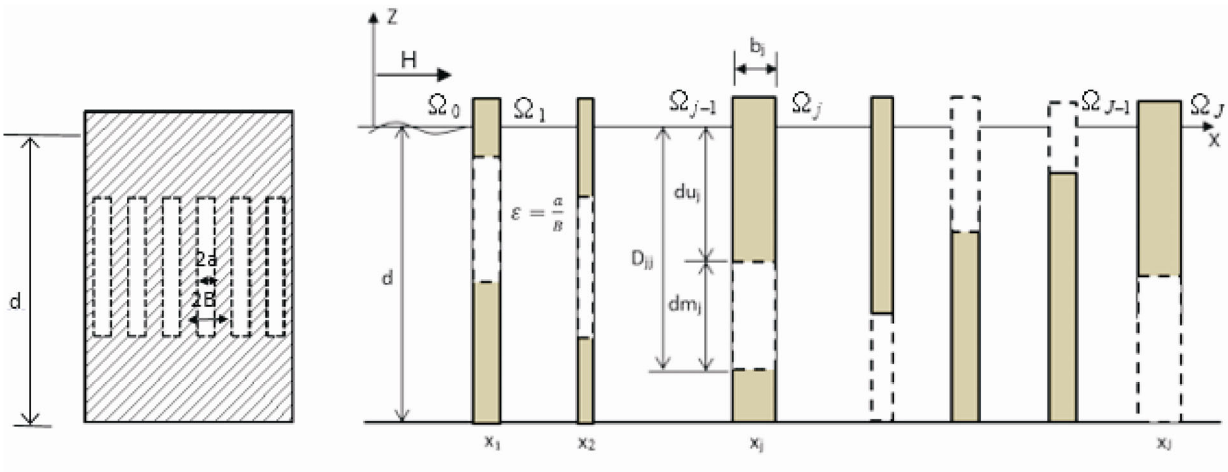

Fig. 1 Definition sketch for a vertical slotted wall breakwater

$$\frac{\partial \Phi_j}{\partial z} = 0, \quad \text{at } z = -d \text{ for } \quad j = 0,1,2,...,J \tag{3}$$

where ω represents the wave angular frequency and g is the gravitational acceleration, assuming periodic motion in time t. As an example of a nonlinear theory, we discuss Stokes second-order theory here; see e.g., Sarpkaya and Isaacson (1981). In Stokes higher-order theory, the velocity potential Φ_j is written as a perturbation series with the following form:

$$\Phi_j(x,z,t) = \text{Re}\left\{ \begin{array}{l} -\dfrac{\mathrm{i}gH}{2\omega}\dfrac{1}{\cosh(\mu d)}\phi_j(x,z)\mathrm{e}^{-\mathrm{i}\omega t} \\ -\dfrac{3\mathrm{i}\pi H}{8T}\left(\dfrac{\pi H}{L}\right)\dfrac{1}{\sinh^4(\lambda d)}\varphi_j(x,z)\mathrm{e}^{-2\mathrm{i}\omega t} \end{array} \right\} \tag{4}$$

in which ϕ_j and φ_j represent the first-order and second-order velocity potentials, respectively, H is the incident wave height, and L is the wavelength. Also, Re{} denotes that the real part of the argument, $\mathrm{i}=\sqrt{-1}$, μ and λ are the wave numbers. We obtain the reduced velocity potentials Φ_j by the eigenfunction expansion method used by both Isaacson *et al*. (1998) and Suh *et al*. (2006). The velocity potentials are expressed in a series with an infinite number of solutions. The solutions to Eq. (1) that satisfy the boundary conditions, Eqs. (2) and (3), are given as follows:

$$\Phi_0 = C_1\cos[\mu_0(d+z)]\mathrm{e}^{-\mu_0(x-x_1)} + C_2\cos[2\lambda_0(d+z)]\mathrm{e}^{-2\lambda_0(x-x_1)} + \sum_{m=0}^{\infty} B_{0m}[C_{1m}\cos[\mu_m(d+z)]\mathrm{e}^{\mu_m(x-x_1)} + C_{2m}\cos[2\lambda_m(d+z)]\mathrm{e}^{2\lambda_m(x-x_1)}] \quad \text{at } x \le x_1 \tag{5}$$

$$\Phi_j = \sum_{m=0}^{\infty} A_{jm}\left[C_{1m}\cos[\mu_m(d+z)]\mathrm{e}^{-\mu_m(x-x_j)} + C_{2m}\cos[2\lambda_m(d+z)]\mathrm{e}^{-2\lambda_m(x-x_j)}\right] + \sum_{m=0}^{\infty} B_{jm}\left[C_{1m}\cos[\mu_m(d+z)]\mathrm{e}^{\mu_m(x-x_{j+1})} + C_{2m}\cos[2\lambda_m(d+z)]\mathrm{e}^{2\lambda_m(x-x_{j+1})}\right] \quad \text{at } x_j \le x \le x_{j+1},\ j = 1,2,...,J-1 \tag{6}$$

$$\Phi_J = \sum_{m=0}^{\infty} B_{Jm}[C_{1m}\cos[\mu_m(d+z)]\mathrm{e}^{-\mu_m(x-x_J)} + C_{2m}\cos[2\lambda_m(d+z)]\mathrm{e}^{-2\lambda_m(x-x_J)}] \quad \text{at } x \ge x_J \tag{7}$$

$$C_1 = -\frac{\mathrm{i}gH}{2\omega}\frac{\mathrm{e}^{-\mathrm{i}\omega t}}{\cos(\mu_o d)}, \qquad C_{1m} = -\frac{\mathrm{i}gH}{2\omega}\frac{\mathrm{e}^{-\mathrm{i}\omega t}}{\cos(\mu_m d)} \tag{8}$$

$$C_2 = -\frac{3\mathrm{i}\pi H}{8T}\left(\frac{\pi H}{L}\right)\frac{\mathrm{e}^{-2\mathrm{i}\omega t}}{\sin^4(\lambda_o d)}, \qquad C_{2m} = -\frac{3\mathrm{i}\pi H}{8T}\left(\frac{\pi H}{L}\right)\frac{\mathrm{e}^{-2\mathrm{i}\omega t}}{\sin^4(\lambda_m d)} \tag{9}$$

where A_{jm} and B_{jm} are the coefficients of the component waves propagating forward and backward, respectively. The first subscript (j) indicates the row of the wall, while the second subscript (m) indicates the wave component. The wave numbers μ_m are the solutions to the first-order dispersion relation, $\omega^2 = -g\mu_m\tan(\mu_m d)$, (Chakrabarti, 1987; Sarpkaya and Isaacson, 1981) and the λ_m values are the solutions to the second-order dispersion relation, $(2\omega)^2 = -g\lambda_m\tan(2\lambda_m d)$. They have an infinite discrete set of real roots $\pm\mu_m$ and $\pm\lambda_m$ ($m\geq1$) for non-propagating evanescent waves and a pair of imaginary roots $\pm\mathrm{i}\mu_0$ and $\pm\mathrm{i}\lambda_0$, respectively, for propagating waves. We take the negative sign so that the propagating waves in Eqs. (5) and (7) correspond to the reflected and transmitted waves, respectively. We also take the positive roots for $m\geq1$ so that the non-propagating waves vanish exponentially with distance from the wall. Eqs. (5)–(7) satisfy all relevant boundaries, and automatically satisfy the requirement that the horizontal velocities must be matched at the breakwater. Velocity potentials are also required to satisfy the following matching conditions:

$$\frac{\partial \Phi_{j-1}}{\partial x}=\frac{\partial \Phi_{j}}{\partial x}=0 \text{ , for } x=x_j, \quad -du_j \le z \le 0, \quad j=1,2,\ldots,J \tag{10}$$

$$\frac{\partial \Phi_{j-1}}{\partial x}=\frac{\partial \Phi_{j}}{\partial x}=0 \text{ , for } x=x_j, \; -d \le z \le -D_j, \; j=1,2,\ldots,J \tag{11}$$

The permeable boundary condition along the slotted wall can be developed based on the formulation of Sollitt and Cross (1972) and adopted by Yu (1995) and Isaacson *et al*. (1998) for a thin vertical barrier:

$$\frac{\partial \Phi_{j-1}}{\partial x}=\frac{\partial \Phi_{j}}{\partial x}=\mathrm{i}G_j\left(\Phi_{j-1}-\Phi_j\right) \tag{12}$$
$$\text{for } x=x_j, \; -D_j \le z \le -du_j, \; j=1,2,\ldots,J$$

Following Yu (1995), G_j is expressed as follows:

$$G_j=\frac{\varepsilon_j}{b_j(f_j-is_j)}=\left|G_j\right|\mathrm{e}^{\mathrm{i}\theta_j}, \quad 0\le\theta_j\le \pi/2 \tag{13}$$

where 'G_j' is a permeability parameter of the jth barrier, which is generally complex and θ_j is the argument of the complex G_j, when $\left|G_j\right|$ equals zero, the perforated wall reduces to an impermeable wall, while for $\left|G_j\right|$ tends toward infinity, the wall becomes entirely transparent. 'b_j' is the barrier thickness, f_j represents the friction coefficient and ε_j is the porosity of the perforated part of the jth wall. In the original formulation of Sollitt and Cross (1972) f_j is calculated implicitly using the Lorentz principle of equivalent work so that the nonlinear effects of wave steepness are retained. In the present study the formulation of Yu (1995) is followed such that f_j is treated simply as a constant which is assumed to be known. s_j represents the inertia coefficient given as follows:

$$s_j=1+C_m\left(\frac{1-\varepsilon_j}{\varepsilon_j}\right) \tag{14}$$

where C_m represents the added mass coefficient, which is treated as a constant. For convenience, the variables are redefined as follows:

$$\begin{aligned} Z_0&=C_1\cos[\mu_0(d+z)], \quad Z_0'=C_2\cos[2\lambda_0(d+z)]\\ Z_m&=C_1\cos[\mu_m(d+z)], \quad Z_m'=C_2\cos[2\lambda_m(d+z)]\end{aligned} \tag{15}$$

and $\Delta x_j=x_{j+1}-x_j$. Substituting Eqs. (5), (6), and (7) into the boundary conditions at the breakwater gives the resulting Eqs. (10), (11), and (12). These are known as series relations, as described by Dalrymple and Martin (1990), and are to be solved for the values of the coefficients. Every third condition can be combined to make one mixed boundary condition that specifies the potential along the z-axis, such that $P(z)$ denotes the boundary condition on the right side of the wall and $Q(z)$ denotes the boundary condition on the left side of the wall as follows:

$$P_1^{-du_1\le z\le 0}(z)=\sum_{m=0}^{\infty}B_{0m}\left[\mu_m Z_m+2\lambda_m Z_m'\right]-\left[\mu_0 Z_0+2\lambda_0 Z_0'\right] \tag{16}$$
$$\text{for } x=x_1, \; -du_1\le z\le 0$$

$$P_1^{-d\le z\le -D_1}(z)=\sum_{m=0}^{\infty}B_{0m}\left[\mu_m Z_m+2\lambda_m Z_m'\right]-\left[\mu_0 Z_0+2\lambda_0 Z_0'\right] \tag{17}$$
$$\text{for } x=x_1, \; -d\le z\le -D_1$$

$$\begin{aligned}P_1^{-D_1\le z\le -du_1}(z)=&\sum_{m=0}^{\infty}B_{0m}\left(\mu_m-\mathrm{i}G_1\right)Z_m+\\ &\sum_{m=0}^{\infty}B_{0m}\left(2\lambda_m-\mathrm{i}G_1\right)Z_m'+\mathrm{i}G_1\sum_{m=0}^{\infty}A_{1m}\left[Z_m+Z_m'\right]+\\ &\mathrm{i}G_1\sum_{m=0}^{\infty}B_{1m}\left[Z_m\,\mathrm{e}^{-\mu_m\Delta x_1}+Z_m'\,\mathrm{e}^{-2\lambda_m\Delta x_1}\right]-\\ &\left(\mu_0+\mathrm{i}G_1\right)Z_0-\left(2\lambda_0+\mathrm{i}G_1\right)Z_0'\end{aligned} \tag{18}$$
$$\text{for } x=x_1, \; -D_1\le z\le -du_1$$

$$Q_1^{-du_1\le z\le 0}(z)=\sum_{m=0}^{\infty}B_{0m}\left[\mu_m Z_m+2\lambda_m Z_m'\right]-\left[\mu_0 Z_0+2\lambda_0 Z_0'\right] \tag{19}$$
$$\text{for } x=x_1, \; -du_1\le z\le 0$$

$$Q_1^{-d\le z\le -D_1}(z)=\sum_{m=0}^{\infty}B_{0m}\left[\mu_m Z_m+2\lambda_m Z_m'\right]-\left[\mu_0 Z_0+2\lambda_0 Z_0'\right] \tag{20}$$
$$\text{for } x=x_1, \; -d\le z\le -D_1$$

$$\begin{aligned}Q_1^{-D_1\le z\le -du_1}(z)=&\mathrm{i}G_1\sum_{m=0}^{\infty}B_{0m}\left[Z_m+Z_m'\right]+\sum_{m=0}^{\infty}A_{1m}\left(\mu_m-\mathrm{i}G_1\right)Z_m+\\ &\sum_{m=0}^{\infty}A_{1m}\left(2\lambda_m-\mathrm{i}G_1\right)Z_m'-\sum_{m=0}^{\infty}B_{1m}\left(\mu_m+\mathrm{i}G_1\right)\mathbf{Z}_m\,\mathrm{e}^{-\mu_m\Delta x_1}-\\ &\sum_{m=0}^{\infty}B_{1m}\left(2\lambda_m+\mathrm{i}G_1\right)Z_m'\,\mathrm{e}^{-2\lambda_m\Delta x_1}+\mathrm{i}G_1\left[Z_0+Z_0'\right]\end{aligned} \tag{21}$$
$$\text{for } x=x_1, \; -D_1\le z\le -du_1$$

$$\begin{aligned}P_j^{-du_j\le z\le 0}(z)=&-\sum_{m=0}^{\infty}A_{j-1m}\left[\mu_m Z_m\,\mathrm{e}^{-\mu_m\Delta x_{j-1}}+2\lambda_m Z_m'\,\mathrm{e}^{-2\lambda_m\Delta x_{j-1}}\right]+\\ &\sum_{m=0}^{\infty}B_{j-1m}\left[\mu_m Z_m+2\lambda_m Z_m'\right]\end{aligned} \tag{22}$$
$$\text{for } x=x_j, -du_j\le z\le 0, \; j=2,3,\ldots,J-1$$

$$\begin{aligned}P_j^{-d\le z\le -D_j}(z)=&-\sum_{m=0}^{\infty}A_{j-1m}\left[\mu_m Z_m\,\mathrm{e}^{-\mu_m\Delta x_{j-1}}+2\lambda_m Z_m'\,\mathrm{e}^{-2\lambda_m\Delta x_{j-1}}\right]+\\ &\sum_{m=0}^{\infty}B_{j-1m}\left[Z\mu_{mm}+2\lambda_m Z_m'\right]\end{aligned} \tag{23}$$
$$\text{for } x=x_j, \quad -d\le z\le -D_j, \quad j=2,3,\ldots,J-1$$

$$\begin{aligned}P_j^{-D_j\le z\le -du_j}(z)=&-\mathrm{i}G_j\sum_{m=0}^{\infty}A_{j-1m}\left[Z_m\,\mathrm{e}^{-\mu_m\Delta x_{j-1}}+Z_m'\,\mathrm{e}^{-2\lambda_m\Delta x_{j-1}}\right]+\\ &\sum_{m=0}^{\infty}B_{j-1m}\left(\mu_m-\mathrm{i}G_j\right)Z_m+\sum_{m=0}^{\infty}B_{j-1m}\left(2\lambda_m-\mathrm{i}G_j\right)Z_m'+\\ &\mathrm{i}G_j\sum_{m=0}^{\infty}A_{jm}\left[Z_m+Z_m'\right]+\mathrm{i}G_j\sum_{m=0}^{\infty}B_{jm}\left[Z_m\,\mathrm{e}^{-\mu_m\Delta x_j}+Z_m'\,\mathrm{e}^{-2\lambda_m\Delta x_j}\right]\end{aligned} \tag{24}$$
$$\text{for } x=x_j, \; -D_j\le z\le -du_j, \quad j=2,3,\ldots,J-1$$

$$\begin{aligned}Q_j^{-du_j\le z\le 0}(z)=&-\sum_{m=0}^{\infty}A_{jm}\left[\mu_m Z_m+2\lambda_m Z_m'\right]+\\ &\sum_{m=0}^{\infty}B_{jm}\left[\mu_m Z_m\,\mathrm{e}^{-\mu_m\Delta x_j}+2\lambda_m Z_m'\,\mathrm{e}^{-2\lambda_m\Delta x_j}\right]\end{aligned} \tag{25}$$
$$\text{for } x=x_j, \quad -du_j\le z\le 0, \quad j=2,3,\ldots,J-1$$

$$Q_j^{-d\le z\le -D_j}(z) = -\sum_{m=0}^{\infty} A_{jm}\left[\mu_m Z_m + 2\lambda_m Z'_m\right] + \sum_{m=0}^{\infty} B_{jm}\left[\mu_m Z_m \,\mathrm{e}^{-\mu_m \Delta x_j} + 2\lambda_m Z'_m \,\mathrm{e}^{-2\lambda_m \Delta x_j}\right] \tag{26}$$

for $x = x_j, \quad -d \le z \le -D_j, \quad j = 2,3,\ldots,J-1$

$$\begin{aligned} Q_j^{-D_j\le z\le -du_j}(z) &= \mathrm{i}G_j \sum_{m=0}^{\infty} A_{j-1m}\left[Z_m \,\mathrm{e}^{-\mu_m \Delta x_{j-1}} + Z'_m \,\mathrm{e}^{-2\lambda_m \Delta x_{j-1}}\right] + \\ &\mathrm{i}G_j \sum_{m=0}^{\infty} B_{j-1m}\left[Z_m + Z'_m\right] + \sum_{m=0}^{\infty} A_{jm}\left(\mu_m - \mathrm{i}G_j\right) Z_m + \\ &\sum_{m=0}^{\infty} A_{jm}\left(2\lambda_m - \mathrm{i}G_j\right) Z'_m - \sum_{m=0}^{\infty} B_{jm}\left(\mu_m + \mathrm{i}G_j\right) Z_m \,\mathrm{e}^{-\mu_m \Delta x_j} - \\ &\sum_{m=0}^{\infty} B_{jm}\left(2\lambda_m + \mathrm{i}G_j\right) Z'_m \,\mathrm{e}^{-2\lambda_m \Delta x_j} \end{aligned} \tag{27}$$

for $x = x_j, \ -D_j \le z \le -du_j, \ j = 2,3,\ldots,J-1$

$$Q_J^{-du_J\le z\le 0}(z) = \sum_{m=0}^{\infty} B_{Jm}\left[-\mu_m Z_m - 2\lambda_m Z'_m\right] \tag{28}$$

for $x = x_J, \quad -du_J \le z \le 0$

$$Q_J^{-d\le z\le -D_J}(\mathrm{z}) = \sum_{m=0}^{\infty} B_{Jm}\left[-\mu_m Z_m - 2\lambda_m Z'_m\right] \tag{29}$$

for $x = x_J, \quad -d \le z \le -D_J$

$$\begin{aligned} Q_J^{-D_J\le z\le -du_J}(z) &= \mathrm{i}G_J \sum_{m=0}^{\infty} B_{J-1m}\left[Z_m + Z'_m\right] + \\ &\mathrm{i}G_J \sum_{m=0}^{\infty} A_{J-1m}\left[Z_m \,\mathrm{e}^{-\mu_m \Delta x_{J-1}} + Z'_m \,\mathrm{e}^{-2\lambda_m \Delta x_{J-1}}\right] + \\ &\sum_{m=0}^{\infty} B_{Jm}\left(\mu_m - \mathrm{i}G_J\right) Z_m + \sum_{m=0}^{\infty} B_{Jm}\left(2\lambda_m - \mathrm{i}G_j\right) Z'_m \end{aligned} \tag{30}$$

for $x = x_J, \ -D_J \le z \le -du_J$

We can use the least squares technique, suggested by Dalrymple and Martin (1990), to determine the coefficients B_{0m}, which requires the minimum values for the following variables:

$$\int_{-d}^{0} \left|P_1(\mathrm{z})\right|^2 \,\mathrm{d}z = \int_{-d}^{0} \left|Q_1(\mathrm{z})\right|^2 \,\mathrm{d}z = 0 \tag{31}$$

Minimizing these integrals with respect to the coefficient B_{0m} leads to the following:

$$\int_{-d}^{0} P_1^*(\mathrm{z}) \frac{\partial P_1(\mathrm{z})}{\partial B_{0m}} \,dz = \int_{-d}^{0} Q_1^*(\mathrm{z}) \frac{\partial Q_1(\mathrm{z})}{\partial B_{0m}} \,\mathrm{d}z = 0, \ m = 0,1,2,\ldots, \tag{32}$$

where $P_1^*(z)$ and $Q_1^*(z)$ are the complex conjugates of $P_1(z)$ and $Q_1(z)$, respectively, and

$$\frac{\partial P_1^{-du_1\le z\le 0}(z)}{\partial B_{0m}} = \left[\mu_m Z_m + 2\lambda_m Z'_m\right] \tag{33}$$

$$\frac{\partial P_1^{-d\le z\le -D_1}(z)}{\partial B_{0m}} = \left[\mu_m Z_m + 2\lambda_m Z'_m\right] \tag{34}$$

$$\frac{\partial P_1^{-D_1\le z\le -du_1}(z)}{\partial B_{0m}} = \left(\mu_m - \mathrm{i}G_1\right) Z_m + \left(2\lambda_m - \mathrm{i}G_1\right) Z'_m \tag{35}$$

$$\frac{\partial Q_1^{-du_1\le z\le 0}(z)}{\partial B_{0m}} = \left[\mu_m Z_m + 2\lambda_m Z'_m\right] \tag{36}$$

$$\frac{\partial Q_1^{-d\le z\le -D_1}(z)}{\partial B_{0m}} = \left[\mu_m Z_m + 2\lambda_m Z'_m\right] \tag{37}$$

$$\frac{\partial Q_1^{-D_1\le z\le -du_1}(z)}{\partial B_{0m}} = \mathrm{i}G_1\left[Z_m + Z'_m\right] \tag{38}$$

Substituting Eqs. (33)–(38) into Eq. (32) yields the following:

$$\begin{aligned} \int_{-d}^{0} P_1^*(\mathrm{z}) \frac{\partial P_1(\mathrm{z})}{\partial B_{0m}} \,\mathrm{d}z = &\int_{-du_1}^{0} B_{0n}^*\left[\mu_n Z_n + 2\lambda_n Z'_n\right]^*\left[\mu_m Z_m + 2\lambda_m Z'_m\right] - \\ &\left[\mu_0 Z_0 + 2\lambda_0 Z'_0\right]^*\left[\mu_m Z_m + 2\lambda_m Z'_m\right]\mathrm{d}z + \\ &\int_{-d}^{-D_1} B_{0n}^*\left[\mu_n Z_n + 2\lambda_n Z'_n\right]^*\left[\mu_m Z_m + 2\lambda_m Z'_m\right] - \\ &\left[\mu_0 Z_0 + 2\lambda_0 Z'_0\right]^*\left[\mu_m Z_m + 2\lambda_m Z'_m\right]\mathrm{d}z + \\ &\int_{-D_1}^{-du_1} B_{0n}^*\left\{\left(\mu_n - \mathrm{i}G_1\right)Z_n + \left(2\lambda_n - \mathrm{i}G_1\right)Z'_n\right\}^*\left\{\left(\mu_m - \mathrm{i}G_1\right)Z_m + \left(2\lambda_m - \mathrm{i}G_1\right)Z'_m\right\} + \\ &A_{1n}^*\left\{\mathrm{i}G_1\left[Z_n + Z'_n\right]\right\}^*\left\{\left(\mu_m - \mathrm{i}G_1\right)Z_m + \left(2\lambda_m - \mathrm{i}G_1\right)Z'_m\right\} + \\ &B_{1n}^*\left\{\mathrm{i}G_1\left[Z_n \,\mathrm{e}^{-\mu_n \Delta x_1} + Z'_n \,\mathrm{e}^{-2\lambda_n \Delta x_1}\right]\right\}^*\left\{\left(\mu_m - \mathrm{i}G_1\right)Z_m + \left(2\lambda_m - \mathrm{i}G_1\right)Z'_m\right\} - \\ &\left\{\left(\mu_0 + \mathrm{i}G_1\right)Z_0 + \left(2\lambda_0 + \mathrm{i}G_1\right)Z'_0\right\}^*\left\{\left(\mu_m - \mathrm{i}G_1\right)Z_m + \left(2\lambda_m - \mathrm{i}G_1\right)Z'_m\right\}\mathrm{d}z = 0 \end{aligned} \tag{39}$$

and

$$\begin{aligned} &\int_{-d}^{0} Q_1^*(\mathrm{z}) \frac{\partial Q_1(\mathrm{z})}{\partial B_{0m}} \,\mathrm{d}z = \\ &\int_{-du_1}^{0} B_{0n}^*\left[\mu_n Z_n + 2\lambda_n Z'_n\right]^*\left[\mu_m Z_m + 2\lambda_m Z'_m\right] - \left[\mu_0 Z_0 + 2\lambda_0 Z'_0\right]^*\left[\mu_m Z_m + 2\lambda_m Z'_m\right]\mathrm{d}z + \\ &\int_{-d}^{-D_1} B_{0n}^*\left[\mu_n Z_n + 2\lambda_n Z'_n\right]^*\left[\mu_m Z_m + 2\lambda_m Z'_m\right] - \left[\mu_0 Z_0 + 2\lambda_0 Z'_0\right]^*\left[\mu_m Z_m + 2\lambda_m Z'_m\right]\mathrm{d}z + \\ &\int_{-D_1}^{-du_1} B_{0n}^*\left\{\mathrm{i}G_1\left[Z_n + Z'_n\right]\right\}^*\left\{\mathrm{i}G_1\left[Z_m + Z'_m\right]\right\} + A_{1n}^*\left\{\left(\mu_n - \mathrm{i}G_1\right)Z_n\right\}^*\left\{\mathrm{i}G_1\left[Z_m + Z'_m\right]\right\} + \\ &A_{1n}^*\left\{\left(2\lambda_n - \mathrm{i}G_1\right)Z'_n\right\}^*\left\{iG_1\left[Z_m + Z'_m\right]\right\} - B_{1n}^*\left\{\left(\mu_n + \mathrm{i}G_1\right)Z_n \,\mathrm{e}^{-\mu_n \Delta x_1}\right\}^*\left\{\mathrm{i}G_1\left[Z_m + Z'_m\right]\right\} - \\ &B_{1n}^*\left\{\left(2\lambda_n + \mathrm{i}G_1\right)Z'_n \,\mathrm{e}^{-2\lambda_n \Delta x_1}\right\}^*\left\{\mathrm{i}G_1\left[Z_m + Z'_m\right]\right\} + \left\{\mathrm{i}G_1\left[Z_0 + Z'_0\right]\right\}^*\left\{\mathrm{i}G_1\left[Z_m + Z'_m\right]\right\}\mathrm{d}z = 0 \end{aligned} \tag{40}$$

Once the wave potentials are calculated, various engineering wave properties can be obtained. The (real) transmission and reflection coefficients, denoted as C_T and C_R, respectively, are defined as the appropriate ratios of the wave heights: $C_T = H_T/H$ and $C_R = H_R/H$, where H_T and H_R are the transmitted and reflected wave heights, respectively (Isaacson *et al*., 1999). These are given in terms of B_{0m} and B_{Jm} as follows:

$$C_R = \left|B_{00}\right| \tag{41}$$

and

$$C_T = \left|B_{J0}\right| \tag{42}$$

To obtain a simple formula for B_{00}, we consider only the propagating wave mode (n=m=0). By substituting n=m=0 in Eq.(39), B_{00}^*, which is the complex conjugate of B_{00}, can be obtained as follows:

$$\begin{aligned}
&B_{00}^*\left\{\int_{-du_1}^{0} k^2\left[Z_0+2Z_0'\right]^*\left[Z_0+2Z_0'\right]\mathrm{d}z+\right.\\
&\int_{-h}^{-D_1} k^2\left[Z_0+2Z_0'\right]^*\left[Z_0+2Z_0'\right]\mathrm{d}z+\\
&\left.\int_{-D_1}^{-du_1}\left\{\left(k+G_1\right)Z_0+\left(2k+G_1\right)Z_0'\right\}^*\left\{\left(k+G_1\right)Z_0+\left(2k+G_1\right)Z_0'\right\}\mathrm{d}z\right\}=\\
&\int_{-du_1}^{0} k^2\left[Z_0+2Z_0'\right]^*\left[Z_0+2Z_0'\right]\mathrm{d}z+\\
&\int_{-d}^{-D_1} k^2\left[Z_0+2Z_0'\right]^*\left[Z_0+2Z_0'\right]\mathrm{d}z+\\
&\int_{-D_1}^{-du_1}\left\{\left(k-G_1\right)Z_0+\left(2k-G_1\right)Z_0'\right\}^*\left\{\left(k+G_1\right)Z_0+\left(2k+G_1\right)Z_0'\right\}\mathrm{d}z
\end{aligned} \tag{43}$$

The energy dissipation through the permeable part of the wall corresponds to the difference in energy between the incident wave and the sum of the energy of the reflected and transmitted waves. The wave energy dissipation coefficient C_E is expressed as follows:

$$C_E = 1 - C_R^2 - C_T^2 \tag{44}$$

The wave force on each wall can be calculated by integrating the wave pressure acting on both the up-wave and down-wave sides of the wall. The magnitude of the horizontal wave force on the unit width of the front wall, F_f, is given as follows:

$$\begin{aligned}
&F_f = \mathrm{i}\rho\omega\int_{-d}^{0}(\Phi_0-\Phi_1)\big|_{x=x_1}\mathrm{d}z =\\
&-\frac{\rho\omega^2 H}{2\mu_0^2}+\sum_{m=0}^{\infty}-\frac{\rho\omega^2 H}{2\mu_m^2}\left(B_{0m}-A_{1m}-B_{1m}\mathrm{e}^{\mu_m(x_1-x_2)}\right)+\\
&\frac{3\rho\omega\pi H}{8T}\left(\frac{\pi H}{L}\right)\left\{\begin{array}{l}\dfrac{\sin(2\lambda_0 d)}{2\lambda_0\sin^4(\lambda_0 d)}+\\ \displaystyle\sum_{m=0}^{\infty}\frac{\sin(2\lambda_m d)}{2\lambda_m\sin^4(\lambda_m d)}\left(B_{0m}-A_{1m}-B_{1m}\mathrm{e}^{2\lambda_m(x_1-x_2)}\right)\end{array}\right\}
\end{aligned} \tag{45}$$

The magnitude of the horizontal wave force on the unit width of the rear wall, F_r, is given as follows:

$$\begin{aligned}
&F_r = \mathrm{i}\rho\omega\int_{-d}^{0}(\Phi_{J-1}-\Phi_J)\big|_{x=x_J}\mathrm{d}z=\\
&\sum_{m=0}^{\infty}-\frac{\rho\omega^2 H}{2\mu_m^2}\left(A_{J-1m}\mathrm{e}^{-\mu_m(x_J-x_{J-1})}+B_{J-1m}-B_{Jm}\right)+\\
&\frac{3\rho\omega\pi H}{8T}\left(\frac{\pi H}{L}\right)\left\{\sum_{m=0}^{\infty}\frac{\sin(2\lambda_m d)}{2\lambda_m\sin^4(\lambda_m d)}\left(A_{J-1m}\mathrm{e}^{-2\lambda_m(x_J-x_{J-1})}+B_{J-1m}-B_{Jm}\right)\right\}
\end{aligned} \tag{46}$$

The dimensionless wave forces, C_{Ff} and C_{Fr}, on the front and rear walls, respectively, are defined as follows:

$$C_{Ff} = \frac{\left|F_f\right|}{\rho g H d} \tag{47}$$

$$C_{Fr} = \frac{\left|F_r\right|}{\rho g H d} \tag{48}$$

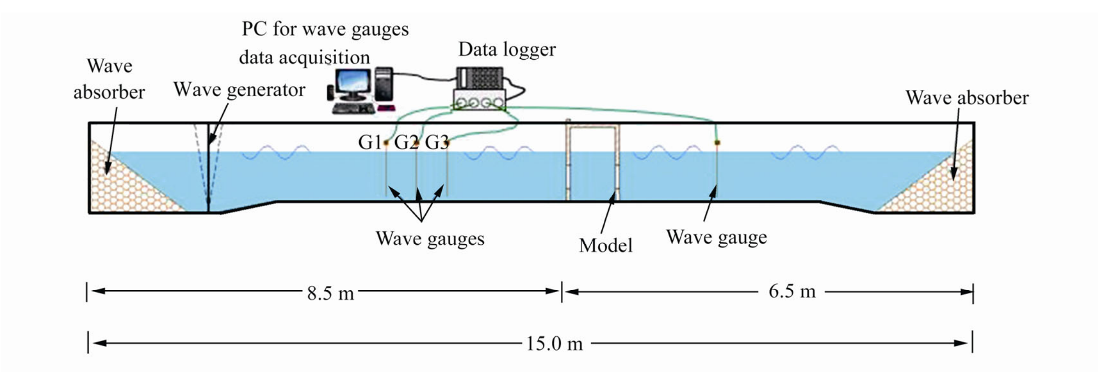

Fig. 2 Experimental setup

Table 1 Specifications of sensors

Sensors type	Blind area/mm	Working range/mm	Frequency/kHz	Techn. Resolution/mm	Reproducibility/%	Output update/Hz	Analogue output/V
USS 635	60	350	400	0.18	±0.15	75	0–10

3 Experimental investigation

We conducted a series of experimental tests on physical models of a double vertical slotted wall with different parameters. The experiments were carried out in the wave flume of the hydraulics laboratory of the Department of Civil Engineering at Umm Al-Qura University, Saudi Arabia. These tests were carried out to measure the wave reflection and transmission coefficients (C_R and C_T) of the proposed double vertical slotted wall using different wave and structural parameters. In addition, we calculated the dissipation coefficients (C_E), as shown in Eq. (44).

3.1 Model scale

In hydraulic model tests of sea waves, the viscosity and surface tension of water do not typically play a significant role in controlling the phenomenon, while inertia and gravity forces are considered to be the predominant governing forces. Thus, we used Froude's law when simulating the studied phenomenon. We used a geometric scale of 1:30 to construct the model of the proposed double vertical slotted wall breakwaters. The selection of this ratio depended on the dimensions of the flume and the wave conditions, i.e., length and height, to be used throughout the experiment.

3.2 Test facility

The flume in the hydraulics laboratory is 15.0 m long, 0.30 m wide, and 0.45 m deep. It is equipped with a wave generator at one end, which is connected to a computer to generate regular waves of different heights and frequencies, and a wave-absorbing slope at the downstream end of the flume. In addition, we constructed a permeable wave absorber to absorb waves generated behind the wave generator to prevent its interference with the main front wave. The details of the experimental setup are shown in Fig. 2. All experiments were conducted at a water depth of 0.3 m and with generator motions corresponding to regular wave trains with different wave periods, ranging from T=0.6 to 1.33 s.

3.3 Model details

The proposed breakwater models basically consist of double vertical slotted walls, which were constructed with vertical panels 0.025 m wide and 0.025 m thick. We varied the porosity of the slotted walls (ε=0.25, 0.33, 0.50, and 0.67) in the middle section. The upper and lower parts are impermeable at different depths, at a ratio based on the water depth. We placed the front vertical barrier to be tested at a fixed distance of 7.5 m from the wave generator and the rear wall was located at various distances from the front wall.

3.4 Wave height measurements

We measured the wave heights using a movable non-contact ultrasonic distance transmitter. This instrument has two main parts: (a) a type USS 635 sensor and (b) an Ultralab ULS 80D. We connected the ultrasonic distance transmitter unit to a computer system to continuously record and store the output data, so that the variation of water surface with time could be plotted. The specification of the type USS 635 sensors are shown in Table 1. The ULS 80D system is equipped with eight fully assembled independent channels, with both an analog output (0–10 V) and a digital RS232 output.

We carried out a static calibration of the wave gauges daily and at the beginning and end of each set of experiments. The calibration constants were found to have a standard deviation of less than 1.0%.

To measure the incident and reflected wave heights at the structure, we positioned three wave gauges in front of the structure (Fig. 2), and used these three gauges to reduce the errors in the amplitudes and phase measurements. Using the three-probe method of Mansard and Funke (1980), we adjusted the spacing between the first three gauges for each of the wave periods to calculate the reflection coefficient. The distance between the first two gauges (X_{12}) in the line of wave propagation was one-tenth of a wave length ($X_{12}=L/10$)). The distance between the first and third wave gauges (X_{13}) in the line of wave propagation should satisfy the following conditions: (a) $L/6<X_{13}<L/3$, (b) $X_{13}\neq L/5$, and (c) $X_{13}\neq 3L/10$. Hence, we selected X_{13} as $X_{13}=L/4$.

Another parameter of similar importance is the distance of the wave gauges in front of the structure. Goda and Suzuki (1976) suggested that gauges be located at least one wave length (wave length corresponding to the peak frequency) (L_{max}=2.0 m) away from the reflective structures.

To avoid the effect of turbulence caused by wave-structure interaction, we measured the wave transmission by the wave gauge at the rear side of the model at a distance of 2.0 m.

To estimate the reflection and transmission coefficients for each test, we used the wave records obtained from the gauges. We estimated the reflection and transmission coefficients using a least-squares method applied to simultaneous measurements of the water surface elevation of the breakwater's up-wave and down-wave. We obtained the incident wave height from measurements without the barriers in place.

4 Validation of proposed mathematical model

To examine the effectiveness of the proposed model, we compared the theoretical predictions of the hydrodynamic coefficients (reflection, transmission, and dissipation coefficients) with those obtained experimentally and numerically by other researches and from the experimental results of our study.

4.1 Comparison of the proposed model with numerical and experimental data (Isaacson *et al.*, 1999)

We validated the proposed mathematical model by comparing its results with the theoretical and experimental results of Isaacson *et al*. (1999) with respect to the hydrodynamic characteristics of double vertical slotted barriers.

In Isaacson *et al*.'s tests, permeable wave barriers were constructed of vertical panels 2.0 cm wide and 1.3 cm thick. The water depth was d=0.45 m, the wave steepness was H/L=0.07, and the half immersed barrier ($dm=0.50d$) had a porosity of ε=5% and spacing of $\Delta x=2.2d$. The friction coefficient was f=2 and the mass coefficient was C_m=0. Fig. 3 shows a plot of the numerical results and test data of Isaacson *et al*. (1999) for the reflection, transmission, and dissipation coefficients (C_R, C_T, and C_E, respectively) and those of the model proposed in this study. In this figure, the C_R, C_T, and C_E are plotted as a function of kdu. As shown in Fig. 3, the results obtained by the proposed model agree well with the numerical and experimental results of Isaacson *et al.* (1999). The C_R increases with an increasing *kdu*, as shown in Fig. 3(a). The opposite trend can be observed for C_T in Fig. 3(b). As shown in Fig. 3(c), C_E increases with an increasing *kdu* until reaching the peak point, and after that it decreases.

4.2 Comparison of the proposed model with numerical and experimental data (Ji and Suh, 2010)

Next, we validated the proposed mathematical model by comparing its results with the theoretical and experimental results of Ji and Suh (2010), with respect to the hydrodynamic characteristics of a triple-row curtainwall–pile breakwater.

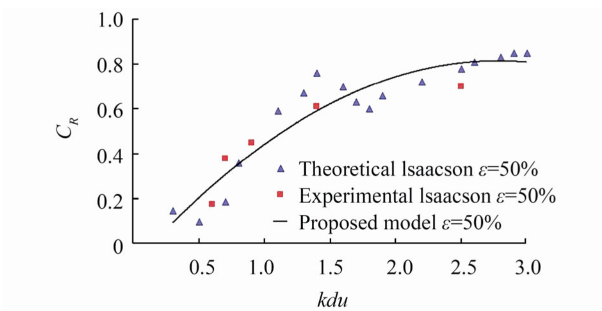

(a) C_R

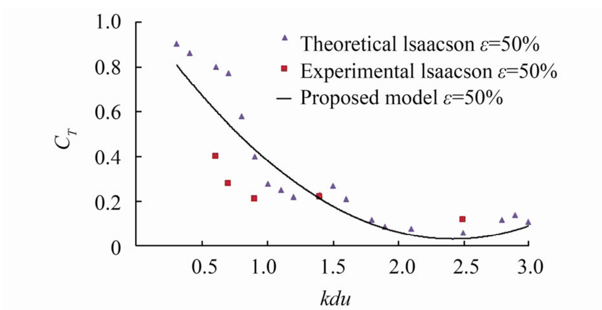

(b) C_T

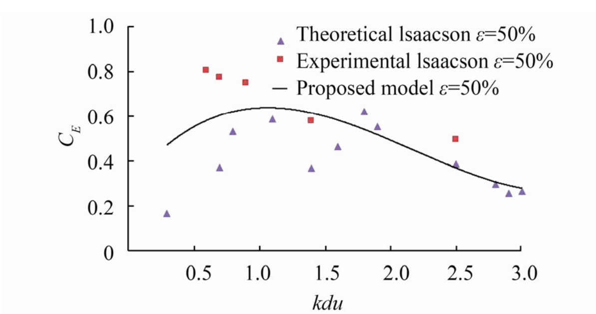

(c) C_E

Fig. 3 Comparison of proposed model results with the theoretical and experimental results of Isaacson *et al.* (1999) for double vertical slotted barriers as a function of *kdu* for ε=5%, *dm*=0.5*d*, Δx=2.2*d*, *f* =2, and C_m=0

The experiments by Ji and Suh (2010) were carried out in the wave flume at the Coastal Engineering Laboratory of Seoul National University, which is 30 m long, 0.6 m wide, and 1 m deep. All experiments were conducted at a water depth of 0.5 m, and square piles with side lengths of 3 cm were used. The draft of permeable part (*dm*=0.5*d*) had a porosity of ε=0.5. The draft of upper curtainwall, *du,* was 0.5*d*. Six different wave periods (*T*=1.0, 1.2, 1.4, 1.6, 1.8, 2.0 s) were used with specified wave heights corresponding to a constant wave steepness of *H*/*L*=0.03. The distance between the first and third rows was 2.0*d*, such that Δx_1=Δx_2=1.0*d*. The friction coefficient was *f*=2 and the mass coefficient was C_m=0. The numerical results and test data of Ji and Suh (2010) for C_R, and C_T and those of the proposed model are plotted in Fig.4. As we can see in the figure, the results obtained by the mathematical model proposed in this study agree well with those of the theoretical and experimental results of Ji and Suh (2010).

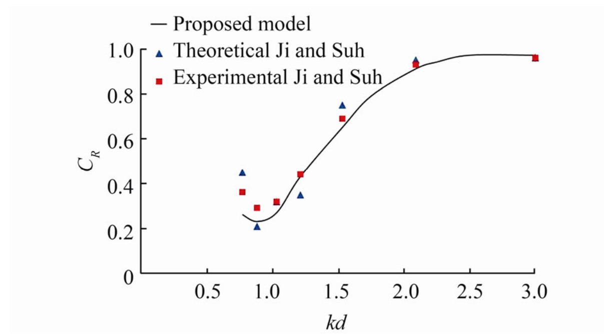

(a) C_R

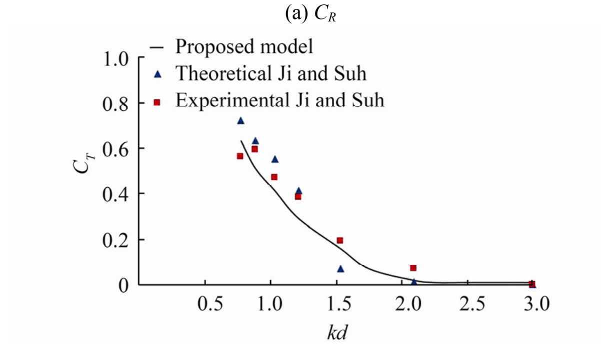

(b) C_T

Fig. 4 Comparison of proposed model results with the theoretical and experimental results of Ji and Suh (2010) for triple-row curtainwall-pile breakwater as a function of *kd* for ε=50%, *du*=0.5*d*, *dm*=0.5*d*, Δx_1=Δx_2=1.0*d*, *f* =2, and C_m=0

4.3 Comparisons with experimental data of the present study

The effects of the permeable wall part *dm* (*dm*=0.8*d*, 0.6*d*, 0.4*d*, and 0.2*d*) on the reflection, transmission, and dissipation coefficients (C_R, C_T, and C_E) of identical double-row walls are shown in Figs. 5, 6, and 7. In these figures, each hydrodynamic parameter is plotted as a function of *kd*. We used three different values for the chamber width Δx=0.5*d*, 1.0*d*, and 2.0*d* in Figs. 5, 6, and 7, respectively. The other calculating conditions used in these figures area porosity of ε=0.5, a friction of *f* =2, and a mass coefficient of C_m=0. From Figs. 5–7, it is evident that the value of the C_R increases with an increasing *kd* at a fixed *dm* and decreases with an increasing *dm* for a fixed *kd.* The C_T follows the opposite trend. The C_E increases with an increasing *kd* until reaching a peak point and then sharply decreases, except in the case of *dm*=0.2*d* and Δ*x*=2.0*d.* The maximum value of the peak C_E increases and moves to the right with an increasing *kd*. Moreover, we can see from Figs. 5, 6, and 7 that with increasing values of Δ*x*/*d*, the C_R decreases monotonically, but a variation of the C_T with an increasing value of Δ*x*/*d* is not noticeable. The C_E and C_R vary oppositely with respect to Δ*x*/*d*.

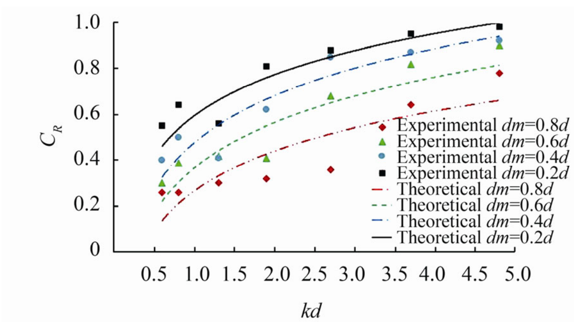

(a) C_R

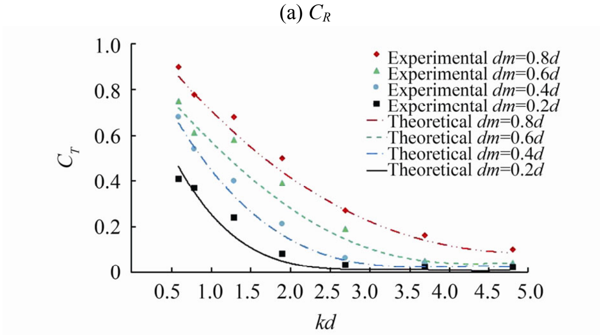

(b) C_T

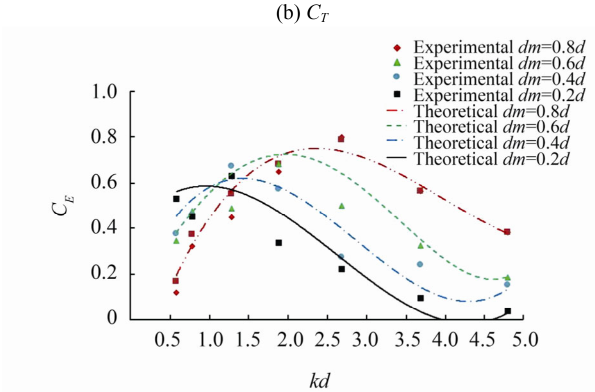

(c) C_E

Fig. 5 Comparison of experimental results with theoretical results as a function of *kd* for four different middle permeable parts of double-row walls with *ε*=50%, Δ*x*=0.5*d*, *f* =2, and C_m=0

In the design of a slotted breakwater, the choice of porosity is particularly important. Fig. 8 presents the measured and predicted hydrodynamic coefficients and the dimensionless wavenumber (*kd*) for different breakwater porosities (*ε*=0.25, 0.33, 0.50, and 0.67) for *f* =2, *cm*=0.00, and *dm*=0.6*d* for double-row walls. The figure shows that the C_R increases with an increasing *kd* and decreases with an increasing porosity *ε*, while the C_T follows the opposite trend. At lower values of *kd*, the decreasing porosity increases the C_E, but for high values of *kd* the decreasing porosity reduces the C_E.

Comparisons of the numerical with the experimental hydrodynamic coefficient results show that the proposed mathematical model can accurately predict the most important features of the experimental results.

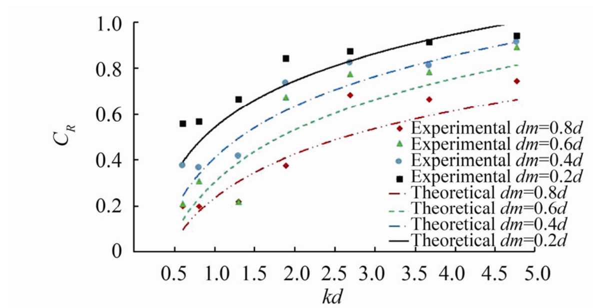

(a) C_R

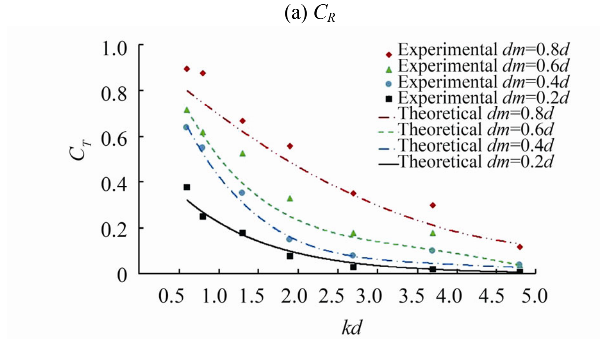

(b) C_T

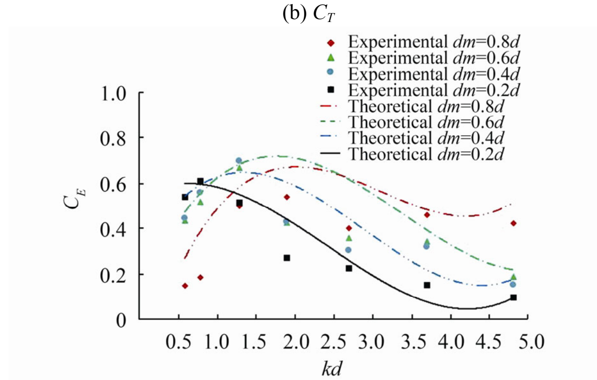

(c) C_E

Fig. 6 Comparison of experimental results with theoretical results as a function of *kd* for four different middle permeable parts of double-row walls with *ε*=50%, Δ*x*=1.0*d*, *f* =2, and C_m=0

5 Numerical examples

Next, we investigated the effect of the permeable wall part *dm* on the hydrodynamic characteristics of the permeable barriers; Fig. 9 shows the behavior of the hydrodynamic characteristics for a double-row wall. As shown in the figure, the C_R, C_T, and C_E values are computed from the new mathematical model as a function of ω^2/gd for various lower permeable wall parts. The porosity ε is 0.5 for the permeable wall part, and the lower permeable wall part *dm* varies from 0.25*d* to 0.75*d.* As such, the draft of the upper impermeable wall part varied according to the *dm*, the friction factor f=2, and the added mass coefficient C_m=0.00. In general, the C_R increases with an increasing ω^2/gd at a fixed *dm,* and increases with a decreasing *dm* for a fixed ω^2/gd. The C_T follows the opposite trend. From Fig. 9(c), we can see that the locations of peak points of the C_E shift toward a larger ω^2/gd as *dm* increases. The C_E rapidly increases with an increasing ω^2/gd until reaching the peak points (0.84, 0.77, and 0.81 for *dm*/*d*=0.25, 0.5, and 0.75, respectively), and after wards sharply decreases.

Fig. 10 shows the predicted hydrodynamic characteristics of the triple-row walls as functions of *kd* for different locations of the permeable wall part *dm*. The distance between the first and third rows was fixed as 2.0*d*, such that Δx_1=Δx_2=1.0*d*, ε =50%, f =2, and C_m=0. Fig. 10(a) shows that the C_R increases with a decreasing *dm* at a fixed *kd* and increases with an increasing *kd* at a fixed *dm.* Fig. 10(b) shows that the C_T follows the opposite trend, where by the C_T increases with an increasing *dm* at a fixed *kd* and decreases with an increasing *kd* at a fixed *dm.* It is obvious that the C_R approaches one as *kd* tends to infinity, whereas the C_T approaches zero as *kd* tends to infinity. Fig. 10(c) shows that the C_E slowly increases with an increasing *kd* for the lower *kd* and reaches its maximum value or peak then decreases slowly with an increasing *kd.* The maximum value of the peak increases and moves to the right with an increasing *dm*.

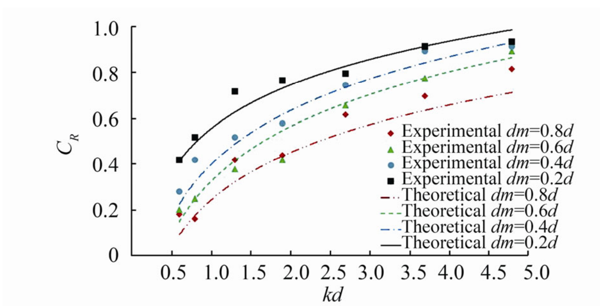

(a) C_R

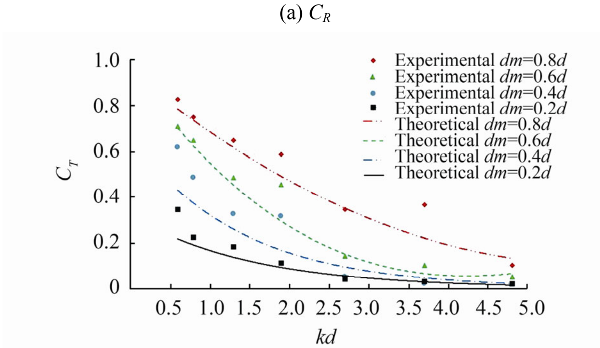

(b) C_T

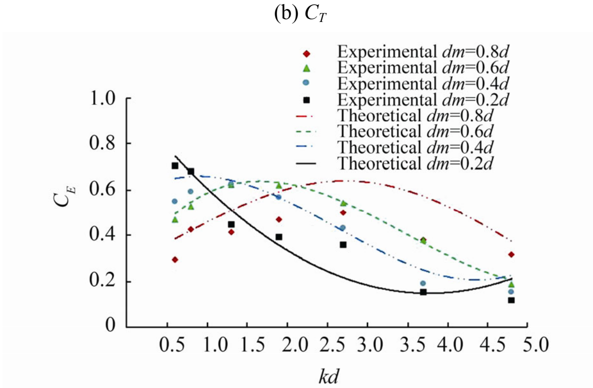

(c) C_E

Fig. 7 Comparison of experimental results with theoretical results for a function of *kd* for four different middle permeable parts of double-row walls with ε=50%, Δx=2.0*d*, f=2, and C_m=0

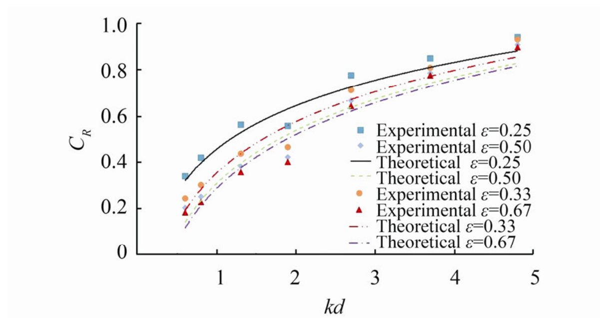

(a) C_R

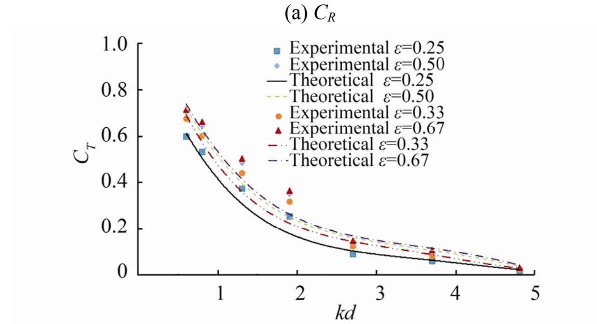

(b) C_T

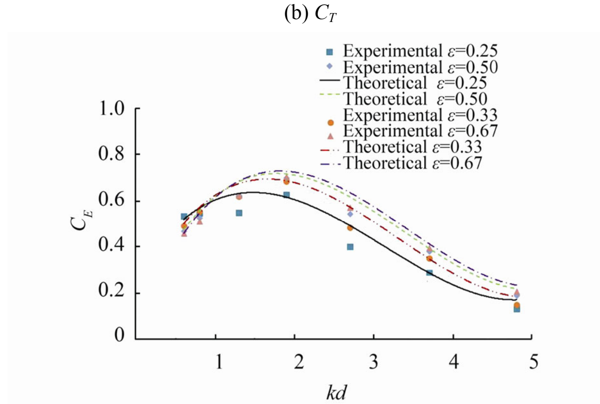

(c) C_E

Fig. 8 Comparison of experimental results with theoretical results for a function of *kd* for different breakwater porosities of double-row walls with d_m=0.6*d*, f=2, and C_m=0

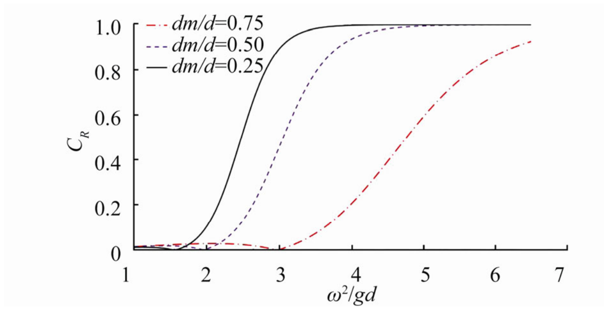

(a) C_R

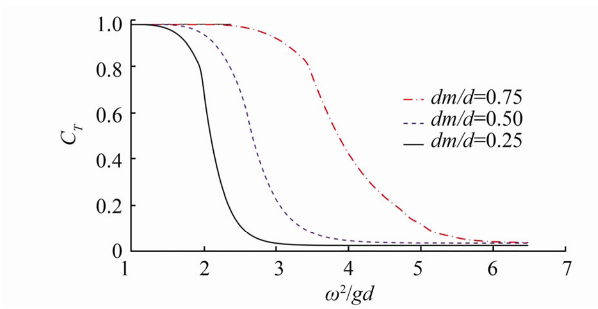

(b) C_T

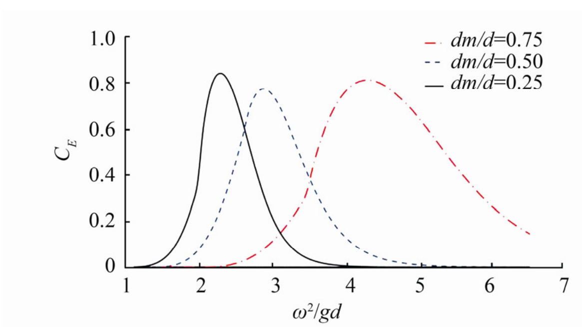

(c) C_E

Fig. 9 Predicted hydrodynamic characteristics computed from the new mathematical model as a function of ω^2/gd for different middle permeable parts of double-row walls with ε=50%, f=2, and C_m=0

Next, we examined the effect of the arrangement of the chamber widths on the C_R, C_T, and C_E values for triple-row walls. Fig. 11 shows comparisons between the widths, or the distance between the walls, and the predicted hydrodynamic characteristics for three different cases of triple-row walls. The dimensions of the all rows were the same. The location of the second wall changed three times between the first and third walls. The first time Δx_1=0.5d, Δx_2=1.5d, the second time Δx_1=1.0d, Δx_2=1.0d, and the third time Δx_1=1.5d, Δx_2=0.5d. We can see from Fig. 11 that the effect of the arrangement of the chamber widths on hydrodynamic characteristics is not very noticeable except for kd<0.5, where the arrangement of the chamber widths significantly affects the hydrodynamic characteristics. In practice, the chambers usually have the same width.

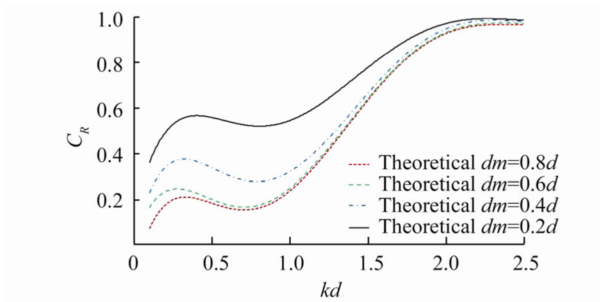

(a) C_R

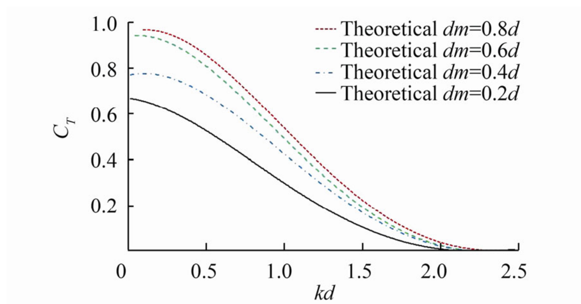

(b) C_T

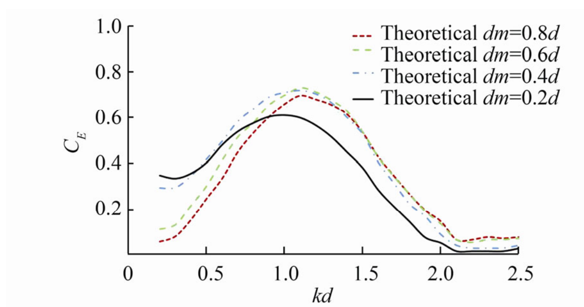

(c) C_E

Fig. 10 Predicted hydrodynamic characteristics computed from the new mathematical model as a function of kd for different middle permeable parts of triple-row walls with Δx_1=Δx_2=1.0d, ε=50%, f =2, and C_m=0

The effects of the number of rows of vertical slotted breakwaters on the horizontal wave force on both the front (C_{Ff}) and rear (C_{Fr}) walls as a function of kd is shown in Fig.12, for ε=50%, du=0.5d, f =2, C_m=0, and Δx=1.0d in double- and triple-row walls. We can see from Fig.12 that when kd>0.5, adopting a double row instead of a single row can significantly reduce the value of C_{Ff}. Obviously, a smaller horizontal wave force would help to enhance the stability of the breakwater. On the other hand, the addition of a third row has very little effect on the value of C_{Ff}. Therefore, triple-row vertical slotted breakwaters would not be recommended unless reducing wave transmission is extremely important. As expected, the horizontal wave force on the rear wall is considerably smaller than on the front wall.

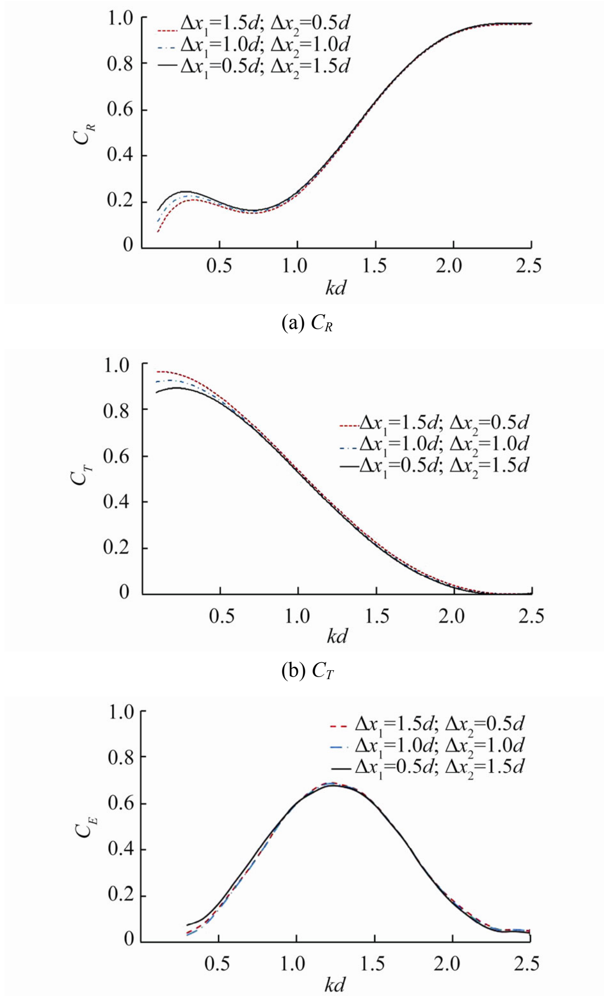

(a) C_R

(b) C_T

(c) C_E

Fig. 11 Predicted hydrodynamic characteristics computed from the new mathematical model as a function of *kd* for various distances between the rows of triple-row walls with middle permeable parts *dm*=0.8*d*, *ε*=50%, *f* =2, and C_m=0

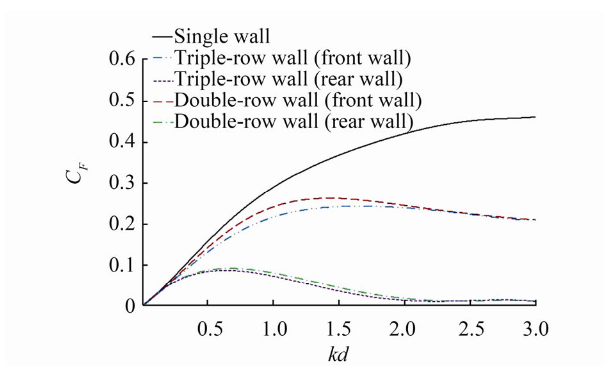

Fig. 12 Comparison between the dimensionless wave force on the front and rear walls on single-row, double-row and triple-row walls computed from the new mathematical model as a function of *kd*, for four different middle permeable parts with *ε*=50%, *du*=0.5*d*, Δ*x*=1.0*d*, *f* =2, and C_m=0

6 Summary and conclusions

Using the eigenfunction expansion method and a least squares technique, in the present study, we developed a mathematical model for Stokes second-order waves to assess the hydrodynamic performance of multiple-row slotted breakwaters. We validated the newly developed solution by comparing its numerical results with respect to several limiting cases with previous predictions. We also validated the correctness of the proposed method by comparing its numerical results with previous experimental data and conducted laboratory tests for further assessment. Comparisons between the measured and predicted results show that the proposed mathematical model agrees well with experimental results. We compared our results with those of experimental measurements of C_R, C_T, and C_E for a partially submerged slotted barrier, and a good agreement was obtained. For double-row slotted breakwaters, the C_R increases with an increasing *kd* at a fixed *dm* and increases with a decreasing *dm* at a fixed *kd.* The C_T follows the opposite trend. The C_E slowly increases with an increasing *kd* for lower *kd* values, reaches a maximum, and then decreases again. On the other hand, the C_R decreases with an increasing *dm/d*, while the C_T follows the opposite trend. The porosity *ε* of the permeable wall part *dm* has a significant influence on the hydrodynamic coefficients, such that increasing *ε* would remarkably decrease the C_R, while increasing the C_T. At lower wave numbers (*kd*), decreasing *ε* increases the C_E, but for high values of *kd*, decreasing *ε* reduces the C_E. On the other hand, for double vertical slotted breakwaters, as the chamber width is relative to increases in the water depth Δ*x*/*d*, the C_R decreases, while a variation of the C_T with an increasing value of Δ*x*/*d* is not noticeable.

These numerical results indicate that for triple-row slotted breakwaters, the effect of the arrangement of chamber widths on the hydrodynamic characteristics is not significant, except when *kd*<0.5, whereby the arrangement of chamber widths has a significant effect. In practice, the chambers usually have the same width. The numerical results also indicate that the horizontal wave force on the front wall is significantly reduced by double-row slotted breakwaters in comparison with single-row slotted breakwaters, for *kd*>0.5. However, the addition of a third row has very little effect on the value of C_{Ff}. As expected, the horizontal wave force on the rear wall is considerably smaller than that on the front wall.

References

Ahmed HG, Schlenkhoff A, Oertel M, 2011. Stokes second-order wave interaction with vertical slotted wall breakwater. *Coastal Structures Conference*, Yokohama, Japan, 691-703.

Balaji R, Sundar V, 2004. Theoretical and experimental investigation on the wave transmission through slotted screens. *Oceanic Engineering International*, **8**(2), 69-90.

Chakrabarti SK, 1987. *Hydrodynamics of offshore structures*. Computational Mechanics Publications, Southampton.

Dalrymple RA, Martin PA, 1990. Wave diffraction through offshore breakwaters. *Journal of Waterway, Port, Coastal and Ocean Engineering*, **116**(6), 727-741.
DOI: 10.1061/(ASCE)0733-950X(1990)116:6(727)

Galal S, 2002. *The use of permeable breakwater for sea defense and shore protection*. Master thesis, Faculty of Engineering, Suez Canal University, Port Said, Egypt.

Gardner JD, Townend IH, 1988. Slotted vertical screen breakwater. *Proceedings Breakwaters*, Eastbourne, 283-298.

Goda Y, Suzuki Y, 1976. Estimation of incident and reflected waves in random wave experiments. *Proceeding of the 15th Costal Engineering Conference*, ASCE, New York, USA, 828-845.

Isaacson M, Baldwim J, Premasiro S, Yang G, 1999. Wave interaction with double slotted barriers. *Applied Ocean Research*, **21**(2), 81-91.
DOI: 10.1016/S0141-1187(98)00039-X

Isaacson M, Premasiri S, Yang G, 1998. Wave interactions with vertical slotted barrier. *Journal of Waterway, Port, Coast and Ocean Engineering*, **124**, 118-126.
DOI: 10.1061/(ASCE)0733-950X(1998)124:3(118)

Ji CH, Suh KD, 2010. Wave interactions with multiple-row curtainwall-pile breakwaters. *Coastal Engineering*, **57**(5), 500-512.
DOI: 10.1016/j.coastaleng.2009.12.008

Koraim A, 2011. Hydrodynamic characteristics of slotted breakwaters under regular waves. *Journal of Marine Science and Technology*, **16**(3), 331-342.
DOI: 10.1007/s00773-011-0126-1

Kriebel DL, 1992. Vertical wave barriers: Wave transmission and wave forces. *23rd International Conference on Coastal Engineering*, Venice, Italy, 1313-1326.

Mansard EPD, Funke ER, 1980.The measurement of incident and reflected spectra using a least squares method. *Proceedings 17th Coastal Engineering Conference*, Sydney, Australia, 159-174.

Sarpkaya T, Isaacson M, 1981. *Mechanics of wave forces on offshore structures*. Van Nostrand Reinhold Company, New York, USA.

Sollitt CK, Cross RH, 1972. Wave transmission through permeable breakwaters. *Proceedings of the 13th Coastal Engineering Conference*, Vancouver, Canada, 1827-1846.

Suh KD, Jung H, Pyun CK, 2007. Wave reflection and transmission by curtainwall-pile breakwaters using circular piles. *Ocean Engineering*, **34**(14-15), 2100-2106.
DOI: 10.1016/j.oceaneng.2007.02.007

Suh KD, Park WS, Park BS, 2001. Separation of incident and reflected waves in wave-current flumes. *Coastal Engineerin*g, **43**(3), 149-159.
DOI: 10.1016/S0378-3839(01)00011-4

Suh KD, Shin S, Cox DT, 2006. Hydrodynamic characteristics of pile-supported vertical wall breakwaters. *Journal of Waterway, Port, Coast and Ocean Engineering*, **132**(2), 83-96.
DOI: 10.1061/(ASCE)0733-950X(2006)132:2(83)

Tsinker G, 1995. *Marine structures engineering specialized Applications*. Chapman and Hall, New York, USA.

Yu X, 1995. Diffraction of water waves by porous breakwaters. *Journal of Waterway, Port, Coast and Ocean Engineering*, **121**(6), 275-282.
DOI: 10.1061/(ASCE)0733-950X(1995)121:6(275)

Zhu ST, Chwang AT, 2001. Investigations on the reflection behaviour of a slotted seawall. *Coastal Engineering*, **43**, 93-104.
DOI: 10.1016/S0378-3839(01)00008-4